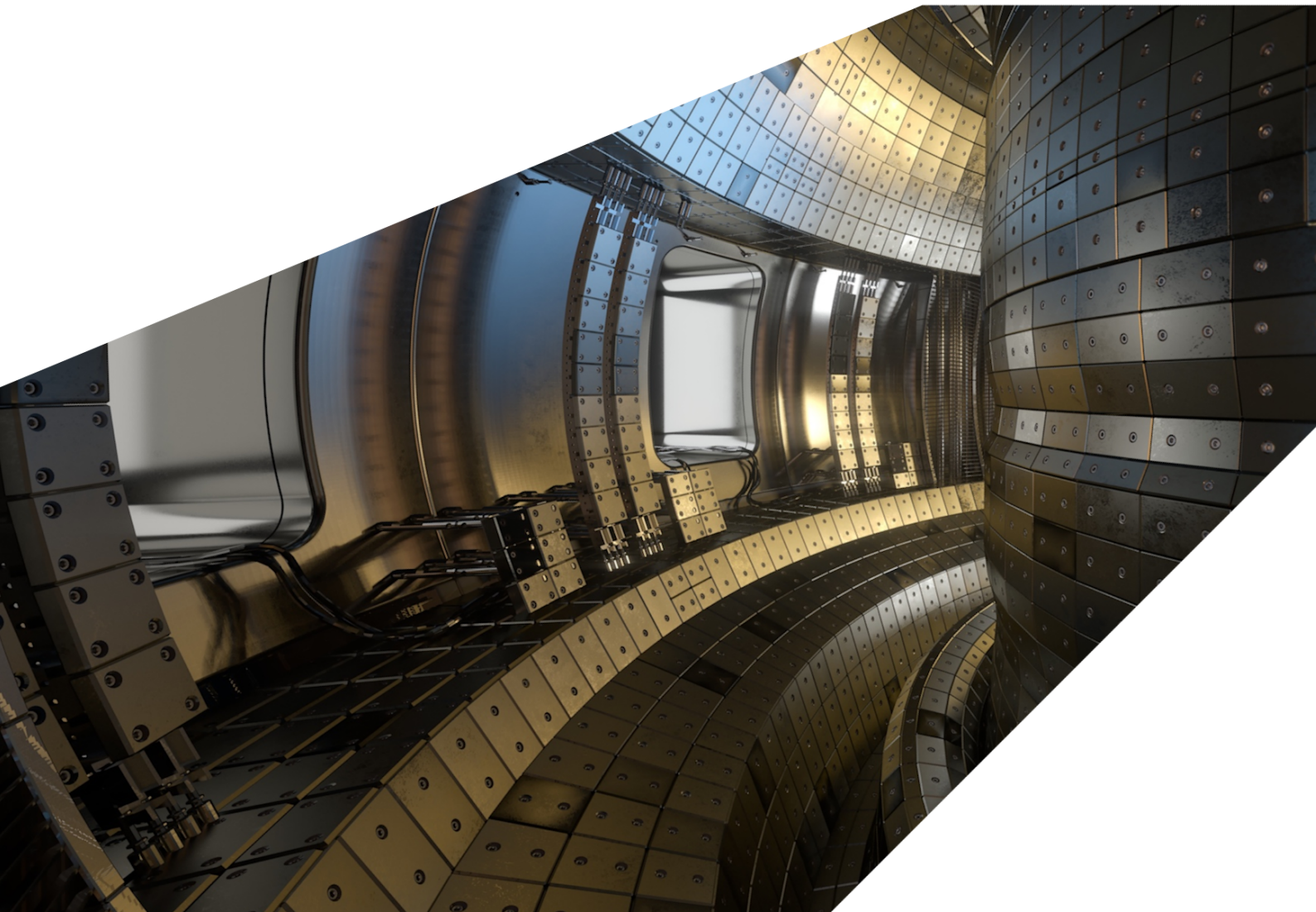**UK Atomic Energy Authority**

ExCALIBUR

Complementary actions. Uncertainty Quantification Code integration, acceptance and operation 1.

M5c.1 Version 1.00

Abstract

The report describes work for ExCALIBUR project NEPTUNE at Milestone M5c.1. It outlines work on uncertainty quantification (UQ) and reduced-order modelling for NEPTUNE. This includes a simple reduced-order model describing convective heat transfer coupled to diffusion, in which one-way and two-way coupling is demonstrated. Two-dimensional heat transfer is studied, with the calculation of a stability boundary between steady and time-dependent solutions. The UQ software EASYVVUQ is applied to a simple test problem in the NESO-PARTICLES framework in anticipation of more complicated examples. Work by the holder of the grant T/AW085/21 is briefly summarized.

UKAEA REFERENCE AND APPROVAL SHEET

	Client Reference:	
	UKAEA Reference:	CD/EXCALIBUR-FMS/0073
	Issue:	1.00
	Date:	27 March 2023

Project Name: ExCALIBUR Fusion Modelling System		

	Name and Department	Signature	Date
Prepared By:	Ed Threlfall Seimon Powell BD	N/A N/A	27 March 2023 27 March 2023
Reviewed By:	Wayne Arter BD		27 March 2023

1   Introduction

Uncertainty quantification (UQ) in NEPTUNE is to be performed non-intrusively, which means that the UQ functionality can be developed largely independently of the main NEPTUNE code base. Since the main NEPTUNE code is still in development, the first part of this report outlines some relevant problems in heat transfer as targets for UQ and presents implementations using the FIREDRAKE PDE solver. The case for this approach is strengthened by the fact that these examples include material on one-way and two-way coupled models (Sec.2) and reduced-order modelling. In addition, the analysis of the three-dimensional version of the heat transfer problem in Sec.3 provides HPC-level problems suitable for use as examples by the holder of the numerical analysis grant T/AW087/22 (specifically, to apply to preconditioners and solution continuation) as well as subjects for UQ campaigns and surrogate construction.

The report also outlines an initial application of the EASYVVUQ software to the NESO-PARTICLES code developed under NEPTUNE (Sec.4).

The UQ work has been defrayed under Grant T/AW085/21. Much of this grantee's work during the past year has taken the form of code development and related hackathons, rather than written reports. This material, which covers UQ, reduced-order models, and data assimilation, is described briefly in Sec.5.

2   Coupled models of heat transport

The experimental campaign of the *SmalLab* programme includes simulations of a convecting fluid in a tank, in which the tank walls have a nonzero thickness and are themselves part of the heat transfer problem, giving a coupled system that is a prime candidate for the application of UQ techniques for studying discrepancies between theoretical models and experimental results. This system is related to the problem of heat transfer in a fusion machine, in which the main challenge is to keep the heat localized where the fusion reactions are intended to occur, see eg. the thesis work of F. Wilczynski and resulting publications such as ref [1]. It is well-known that the rate of heat transfer in a fluid is enhanced by turbulence and so one worthwhile goal is to control and suppress turbulence. The latter can be achieved by reducing the temperature gradient across the fluid region by adding insulation (large gradients are the drivers of turbulence).

Work is currently in progress to enable the coupling of the incompressible Navier-Stokes solver and the diffusion solver of NEKTAR++ in order to enable the simulation of a fluid region (tank interior) coupled to a solid conducting model (tank wall). These modifications are not completed at the time of writing and so a reduced model of heat transfer by turbulent fluids and conductors, and their coupling, is considered.

The study begins by examining a one-dimensional toy system with heat moving from left to right, with temperature equal to unity on the left and zero on the right. Let there be two conducting regions, each of unit width and of thermal conductivity κ_1 (left) and κ_2 (right). The law determining the effective conductivity κ of the composite is
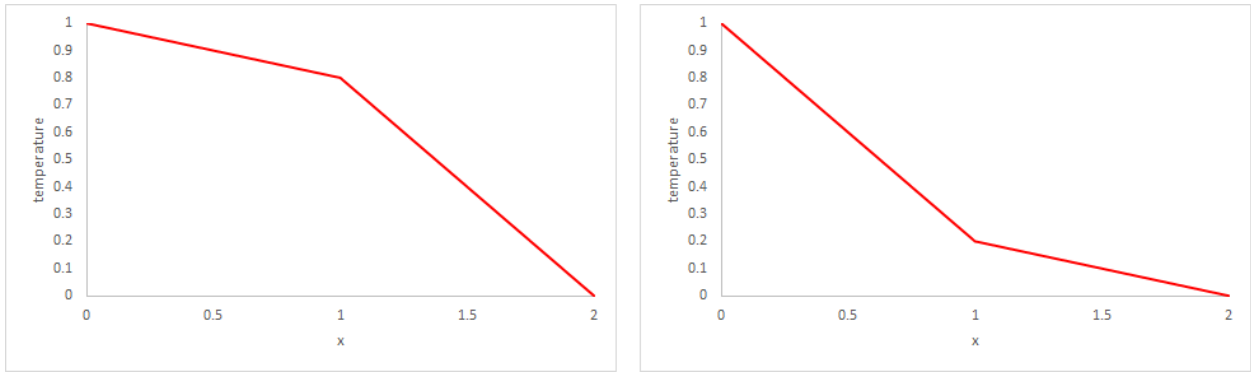
Figure 1: Temperature profile across a composite region with thermal conductivities κ_1 for $x < 1$ and κ_2 for $x > 1$. The left-hand plot shows the case $\kappa_1 = 4\kappa_2$ and the right $4\kappa_1 = \kappa_2$.

$$\kappa = 2\,\frac{\kappa_1\kappa_2}{\kappa_1 + \kappa_2} \tag{1}$$

reminiscent of the law for the combination of electrical resistances in parallel, except for the extra factor of 2.

The heat flux through the combined system is

$$F = \frac{\kappa_1\kappa_2}{\kappa_1 + \kappa_2} \tag{2}$$

(which is symmetric under the interchange of κ_1 and κ_2).

The temperature at the midpoint is

$$T_{mid} = \frac{\kappa_1}{\kappa_1 + \kappa_2} \tag{3}$$

(which is *not* symmetric under the interchange of κ_1 and κ_2).

The midpoint temperature is greater than $\frac{1}{2}$ if $\kappa_1 > \kappa_2$, in which case most of the temperature drop occurs across the second (ie. the rightmost) region ie. the temperature gradient across the first region is reduced (see Fig.1). If the first region is actually a tank of fluid, this means that the Rayleigh number for the convective system will be decreased the poorer conductor the second region is - the fluid will be hotter on average but the temperature gradient across it will be reduced. This means the fluid is less likely to be turbulent, and, given the usual laws for heat transfer by fluids, will transport heat at a lesser rate.

2.1 One-dimensional models - one-way coupled

The model of this section and the next will consist of a zero-dimensional (ie. ODE) surrogate for the convecting fluid, coupled to a one-dimensional diffusion model.

A proxy for the potentially turbulent fluid is the Lorenz equations, also known as the *Lorenz '63 model* [2], obtained by considering Rayleigh-Bénard convection and retaining only the first trigonometric eigenmode associated with departure from the purely-conducting state and its quadratic self-interaction.

The equations are

$$
\begin{aligned}
\dot{X} &= \sigma(Y - X); \\
\dot{Y} &= \rho X - Y - XZ; \\
\dot{Z} &= -\beta Z + XY.
\end{aligned}
$$

$$(4)$$

This model retains some of the characteristics of a turbulent fluid problem ie. it exhibits smooth behaviour for some parameter choices and chaotic behaviour for others. In addition, two of the three free parameters in the model, respectively ρ and σ, correspond to the Rayleigh (Ra) and Prandtl (Pr) numbers derived from the progenitor problem (the remaining parameter, β, is of lesser interest in this study). As a reminder, the Rayleigh number is the dimensionless temperature difference (eg. between the hot and cold sides of a fluid-filled cavity) driving the convection and the Prandtl number is the dimensionless ratio of momentum diffusivity to thermal diffusivity. It is possible to extract the quantity which in the full problem represents the Nusselt number (ie. the rate of heat transfer) as $\mathrm{Nu} = 1 + \frac{2Z}{\rho}$. The Lorenz model is itself an useful candidate for UQ studies due to its simplicity (three parameters) and the fact that its response surfaces may exhibit discontinuous behaviour [3].

A simple C++ ODE solver implementation of the Lorenz model was written. A canonical choice was made for the model parameters $\rho = 28$, $\sigma = 10$, $\beta = \frac{8}{3}$; this choice is one that enables chaotic behaviour. (More generally, the paper [3] exposes the behaviour of the system in $(\mathrm{Ra}, \mathrm{Pr})$-space as an interesting 'phase diagram'.) The outputs are a plausible representation of the familiar Lorenz system behaviour (Fig.2) and this was deemed sufficient as a unit test.

The diffusion model is a simple implementation of a time-dependent diffusion across a one-dimensional domain of unit width. The code was written in C++ and follows the unconditionally-stable implementation in [4] (which uses forward spatial differences and a Crank-Nicolson time-stepping method). The solver can use Dirichlet or Neumann boundary conditions and a simple unit test of the former case against analytic results was performed: the solver was run for $t = 0.1$ using $D = 0.1$, starting from zero temperature everywhere in the volume and $T(x = 0) = 1$, $T(x = 1) = 0$ Dirichlet conditions. The analytic temperature profile is

$$
T(t, x) = 1 - x - \sum_{n=1}^{\infty} \frac{2}{\pi n} e^{-n^2 \pi^2 D t} \sin n\pi x. \tag{5}
$$

(This tends to the obvious steady-state solution $1 - x$ as $t \gg D^{-1}$ and the subtraction is at $t = 0$ simply the Fourier series for that function; the Fourier modes each decay on a timescale set by the wavenumber; the function can be approximated for $t \ll D^{-1}$ by $1 - \mathrm{erf}(\frac{x}{\sqrt{4Dt}})$ which is the solution
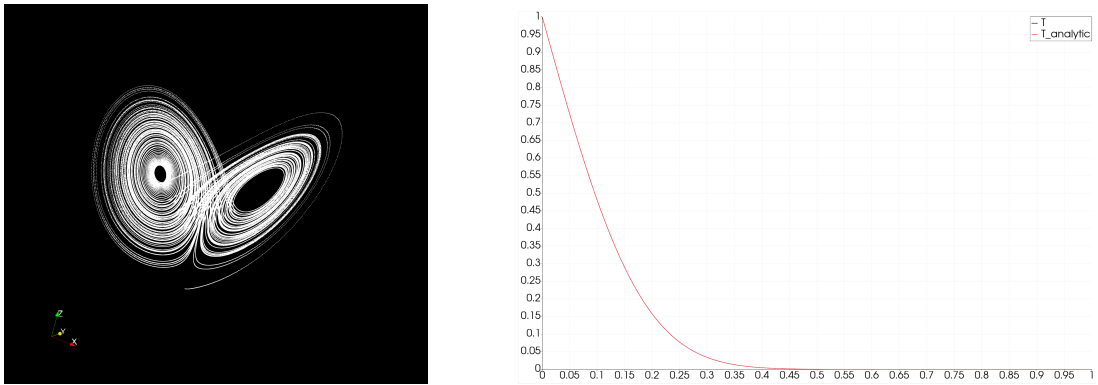
4

Figure 2: (Left) output of Lorenz ODE solver displaying the well-known Lorenz attractor. (Right) unit test of the output of the diffusion solver against theory; there is no visible discrepancy between the code output and the theory curve.
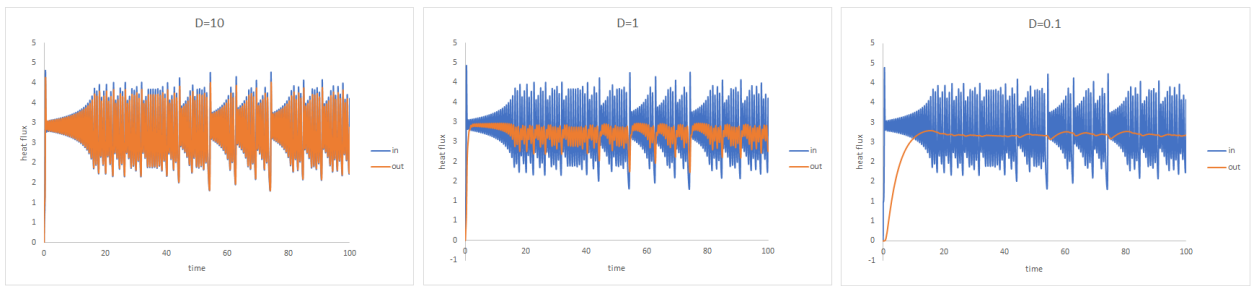

Figure 3: Behaviour of the coupled Lorenz-diffusion system as the diffusivity is varied. The time series used is the heat flux. The conducting region acts as basically a low-pass filter on the heat flux time series.

to the same problem on a semi-infinite interval. These analytic forms agree with the code outputs in Fig.2.)

In the coupled system, the Nusselt number from the Lorenz model is used to provide a Neumann boundary condition on the left-hand side of the diffusion problem (specifically the value of $\frac{\partial T}{\partial x}$ is set equal to $\frac{\text{Nu}}{D}$). The other side of the domain of the diffusion problem (this domain is called the conducting region) is given a homogeneous Dirichlet condition ($T = 0$). The behaviour of the coupled system for different values of diffusivity is show in Fig.3.

There is no coupling of the diffusion model back into the Lorenz model - this would be valid only in the trivial limit where the solid is a much better conductor than the fluid (ie. the temperature is near-uniform across the solid).

2.2 One-dimensional models - two-way coupled

Two-way coupling is necessary in order to study the effect of the insulation on the fluid system.

The diffusion problem can be made to back-react on the Lorenz model by allowing the temperature

5

T_L at the entry point to the conducting region to determine the Rayleigh number ρ in the Lorenz model (recall that for vertical natural convection the Rayleigh number is the non-dimensionalized temperature difference horizontally across the cavity). The connection needs to be made via some function that avoids pathological behaviours; reasonable properties would seem to be that ρ decreases monotonically with increasing T_L and that ρ cannot become negative (this means the minimum Nusselt number is 1 and there cannot be less-than-unity heat fluxes). In practice, a function that ensures $\rho \geq 1$ appears to work better than one that is allowed to decrease to zero, giving better numerical stability and avoiding features such as negative temperatures in the conducting region, heat flux from right to left, and large 'spikes' in heat flux. The function $\rho = 1 + 27e^{-T_L}$ was chosen empirically and was found to give no obvious numerical difficulties; for the initial condition $T_L = 0$ this choice represents the same parameter values as used in the previous section. (Note that, with this function and positive temperatures, the Rayleigh number has a maximum value of 28.) *It seems likely that there are more sensible choices of this function as not much experimentation was done with other choices - work was stopped once a bounded-response choice was found. Note possible similarity to the activation functions chosen in neural networks.*

The parameters σ and β take the same fixed values as in the previous section.

Outputs can be seen in Fig.4; these are the time series for the heat flux into and out the other side of the diffusive region. It can be seen that for large values of D the coupled response preserves well the no-coupling input heat flux (the diffusion is rapid, therefore the temperature is near-uniform - indeed near-zero - across the diffusive region). Small values of D result in a 'turning off' of the turbulence, which physically is supposed to represent the fact that insulating the turbulent region reduces the temperature gradient across it (the fluid is hotter but recall that turbulence is driven by temperature *gradients*) - one sees that the turbulent time series is brought into a quiescent state and the heat flux (Nusselt number) tends to unity, which is the minimum possible rate of heat transfer in this model, corresponding to pure conduction. In between these regimes there is an oscillatory regime (amusingly, this sort of thing is seen in the transition to turbulence in real systems) in which, strangely, the average heat flux is enhanced over the turbulent case - it is expected that this non-monotonicity reflects the non-physical nature of the model, either from the extrapolation of the Lorenz single-mode approximation beyond its region of validity or from the empirical choice of coupling function. It is clear that it is in reality not possible to enhance heat flux by adding further insulation in a one-dimensional system. (Though note that this is not true in higher dimensions; consider heat sinks.)

It is also possible to visualize how the back-reaction affects the behaviour of the Lorenz oscillator (Fig.5). The interesting thing here is the recovery of the usual sort of Lorenz attractor for large values of D, and apparently simpler attractors for reduced values of D, down to fixed points for sufficiently small D. Note that the intermediate attractors display nonmonotonicity in D as to whether they are able to access both 'lobes' of the original Lorenz attractor.

There is scope for further investigation of simple models of this sort (note the compute times for all the examples above are typically one second or less on a single core of a laptop). It is possible to imagine simple control strategies by varying the temperature used as the Dirichlet boundary on the right-hand side of the conducting region. It is possible to imagine coupling additional 'convecting', ie. Lorenz, systems and additional conducting regions.
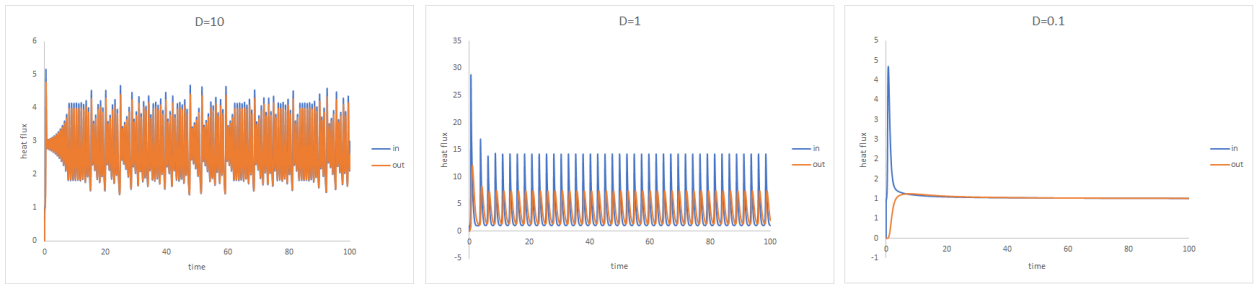
Figure 4: Time series heat flux inputs (blue) and outputs (orange) for the conducting region of the coupled Lorenz and diffusion model for various values of the diffusivity D, ie. the heat flux entering the diffusive region from the turbulent model, which is affected by the back-reaction of the diffusion problem on the Lorenz series in the way explained in the main text. The main phenomenon of interest is the fact that sufficient insulation (small D) results in suppression of the chaotic behaviour, which is interpreted loosely as the suppression of turbulence. Note the plots are not shown here but the time series for the temperature at the left-hand side of the conductor show similar time-dependence, and the average entry temperature seems to be a monotonically-decreasing function of D, which is physically consistent.
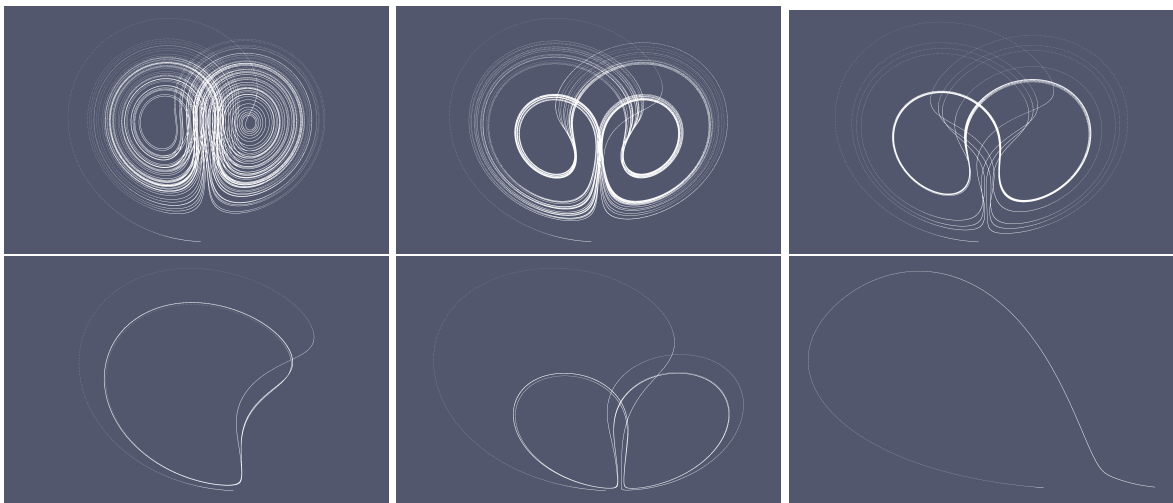

Figure 5: (Modified) Lorenz attractor part of the two-way coupled Lorenz and diffusion model for various values of the diffusivity D. Top (L-R) $D = 10, 4, 3.16$; bottom $D = 2, 1, 0.1$. Note the attractor is largely as in the classic non-coupled case for $D = 10$ and it degenerates to a single figure-of-eight attractor track as D is reduced to 3.16. Below about 3.13 the attractor is confined to one lobe of the classic structure, but this behavior changes with the $D = 1$ case exploring two lobes. Very small values of D lead to the attractor becoming a fixed point with $Z = 0$ corresponding to a pure conducting $\mathrm{Nu} = 1$ situation. All cases are 2-D projections with the positive X-axis oriented into the page (and right-handed Cartesian axes).

The implementation used to generate the results in this section is tightly coupled but there is no reason, other than convenience, not to use a value-passing approach to couple separate Lorenz and diffusion software modules.

3   Convection models as proxyapps for UQ

Attention is now shifted to study of two-dimensional convecting fluids as targets for UQ and reduced-order models.

The well-cited paper [5] presents a 'phase diagram' charting the expected behaviour of Rayleigh-Bénard convection as a function of the two parameters Ra and Pr. The diagram is reproduced here as Fig.6. The analysis in that paper is possible due to a systematic theory based on analytic results for global averages of kinetic and thermal dissipation rates (eg. Eqs.2.5, 2.6 in [5]). This allows consideration of the system behaviour depending on whether the boundary layer or the bulk dominates the kinetic and thermal dissipation and on whether the kinetic or thermal boundary layer is thicker. The case of vertical natural convection (also known as side-heated or slot convection), in which the temperature gradient is applied horizontally, is more challenging as the same approach does not work (the global relations for dissipation rates do not exist). There does not seem to exist in the current literature a vertical natural convection analogue of the diagram in [5], motivating a study of this system. Note that phase transitions are interesting from a UQ standpoint, not least because a small uncertainty in a control parameter value can lead to a very large change in the physical response of the system in the vicinity of a phase boundary (or, in the case in [5], a boundary between two scaling regimes).

The vertical natural convection problem is directly relevant to the *SmalLab* experiments, and it is of interest in the context of uncertainty quantification, as will now be discussed. This work provides an opportunity to test the impact of parameter uncertainty in an interesting model that possesses different physical regimes which furthermore may be demarcated by boundaries at which the response or its derivatives are discontinuous. (A discontinuous response poses a challenge for polynomial fitting techniques which tend to work well only in rather smooth cases.) There is also opportunity to construct useful surrogates of response surfaces that depend on potentially large amounts of computation - the examples presented here will be two-dimensional, but the three-dimensional versions are a supercomputer-level challenge. Even the two-dimensional case is helpful in highlighting some features of the computation that are germane to the construction of the ensemble-based campaign that is necessary in order to perform non-intrusive UQ. Namely:

- UQ campaigns generally aim to achieve a meaningful coverage of a parameter space of some dimensionality, size, and shape. In many cases, coverage is achieved by trivial parallelization of individual calculations. However, it is sometimes advantageous, or even essential, to perform the computations in some sort of ordered pattern - the 'continuation' approach to solving elliptic problems means that the next calculation may need the results from an earlier one from nearby in parameter space (eg. to provide the initial guess) and so some degree of serialization is mandated.

- A specific example of the above is the performance of numerical eigensolvers, which can
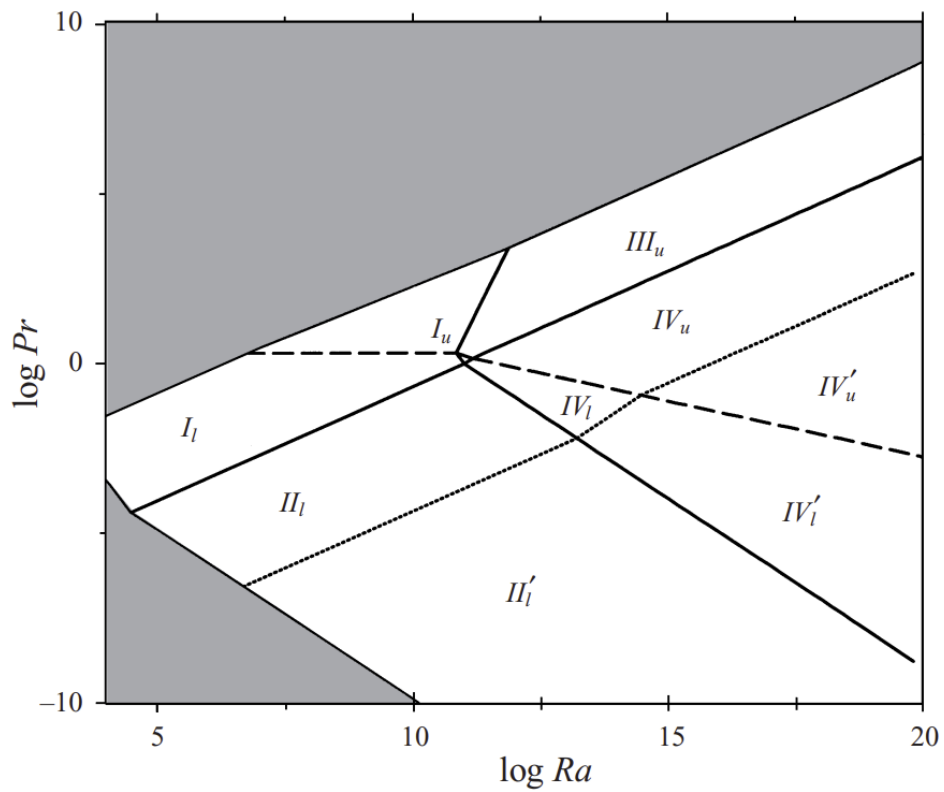
8

Figure 6: The phase diagram of Rayleigh-Bénard convection (Fig.2 in [5]). The differently-labelled regimes correspond to a different scaling law of the Nusselt number (and / or Reynolds number) with Rayleigh and Prandtl numbers $\mathrm{Nu} \sim \mathrm{Ra}^{\alpha}\mathrm{Pr}^{\beta}$.

depend strongly on the initial guess of the eigenvalue. This value can come, as above, from a nearby solution.

- A reduced-order model can be used to inform initial values of the type mentioned above, for example it may be known how an eigenvalue is expected to scale with a control parameter. The need for expensive solution continuation may be removed by using a reduced-order model to initialize the solver at an arbitrary point in parameter space.

- One might consider a simple line-based ordering of simulations in order to achieve coverage of a multi-dimensional parameter space, though this is at odds with Latin-hypercube type approaches. An alternative is to consider placing simulation attempts along a space-filling curve (eg. the Hilbert curve).

- An alternative to serialization is to store the state of previous simulations and to make this data available to solvers performing new simulations (data from a 'nearby' past run could be used as an initial state). This approach would favour algorithms where a large amount of arithmetic work is needed per unit of stored state data.

- As a general principle, understanding gained using a two-dimensional fluid system may be applied to a larger study of the three-dimensional problem and may specifically reduce the amount of trial-and-error needed when working with expensive supercomputer runtime.

It is possible to use NEKTAR++ to obtain the Nusselt number as a function of position in $(\mathrm{Ra}, \mathrm{Pr})$ space. A general analysis is challenging due to the need to tune the parameters of the simulation in order to preserve numerical stability and to ensure that the results are not contaminated by transients. It is expedient to start on the problem using the FIREDRAKE PDE solver framework [6] to solve for the steady state and this is the approach taken here. With the use of a time-independent solver, only the conducting and laminar convecting regimes are accessible. What can usefully be determined from such analysis is the onset of linear instability in the laminar solutions - this gives a bound on the stability of the laminar regime as there the system transitions to an oscillatory solution, which tends to lie between the laminar and turbulent regimes, in what is referred to as a Hopf bifurcation. (The transition to turbulence occurs at higher Ra and is associated to the excitation of many incommensurate linear modes.) The goal then is the discovery of a one-dimensional stability frontier between stationary and oscillatory states in the $(\mathrm{Ra}, \mathrm{Pr})$ plane.

The stability of a given stationary laminar solution is studied by determining the most negative eigenvalue for a linear perturbation about the laminar convecting background states. The criterion for a linear instability is that the real part of the eigenvalue is negative. Here the eigen-analysis is done with the aid of the SLEPc eigensolver library [7]. Two techniques were tried:

- Simple scans of $(\mathrm{Ra}, \mathrm{Pr})$ space to determine where eigenvalues with negative real parts occur.

- A nonlinear analysis technique to determine directly the value of Ra at which the system exhibits a Hopf bifurcation. The method is outlined in a paper by Griewank and Reddien [8]. The FIREDRAKE implementation, which will not be detailed here, was largely copied from [9] with minor differences, eg. in the pressure condition where [9] evades the constant-pressure null space by fixing the pressure at a boundary point, while the present study used the `nullspace` feature of FIREDRAKE.

The scripts here employ a direct solver for the linear systems as in [9]. This is expedient and is effective for small problems but uses more memory than iterative-based approaches. Note that convergence failures here mentioned refer to failure of nonlinear algorithms to converge, rather than the direct linear solver.

One complicating factor is the need to perform solution continuation in order to cover the necessary regions of parameter space (if this is not used, then it is likely that only a small part of the laminar-to-non-stationary stability frontier can be found).

It might be noted that this system is known to exhibit a rich variety of instability phenomena eg. internal gravity waves, instabilities at the corners, and instabilities at the walls; see the literature cited in the sequels for details. A few useful test cases are available in the literature; these are outlined in the following subsections in order to provide some verification of the methods.

3.1 Rayleigh-Bénard convection

The simplest test is to obtain the stability limit of the Rayleigh-Bénard problem. It is well-known that the infinite layer version of this problem becomes unstable to convection at $\mathrm{Ra_c} \approx 1708$ ([10]) and textbook that the Lorenz equations capture its behaviour close to onset correctly as a pitchfork bifurcation (see [11, § 11.2]). Here, it is easier to perform the analysis for a unit square cavity with no-slip boundary conditions at all walls and insulating (the term 'adiabatic' is equivalent) vertical walls. The paper [12] by Farrell et al. contains an analysis of this problem and there a value of $\mathrm{Ra_c} = 2586$ is found using a 50×50 element mesh of uniform squares with order-2 elements used to discretize the velocity and order-1 for the pressure and temperature (called Taylor-Hood elements). Note that the aforementioned paper uses $\mathrm{Pr} = 1$, though in fact the value of the critical Rayleigh number does not depend on the value of the Prandtl number because the background state does not depend on that value.

A Griewank-Reddien analysis was done using FIREDRAKE and starting the eigenvalue search from a value of 2550. Note that the background state for this problem is trivial - a linear variation in temperature from $T = 1$ at the bottom to $T = 0$ at the top, with the appropriate pressure gradient, and zero fluid velocity.

The results (Table 1), obtained using a 50×50 element mesh of uniform squares, show good agreement with those of [12]. The instability mode is illustrated in Fig.7.

3.2 Vertical natural convection with unit aspect ratio

Of course, the R-B problem is simpler and numerically easier than the vertical convection case since the former involves a perturbation to a trivial, non-moving background solution. The vertical case is more challenging as a moving solution appears for at a very small value of the Rayleigh number and the moving background means both that the position of the Hopf bifurcation depends on the value of the Prandtl number, and that the eigenvalue of the first instability mode is not purely real. The nontrivial background also introduces local anisotropy into the system (in the directional flow, that is, *not* anisotropic diffusion).

Author	element orders	$\mathrm{Ra_c}$ value
Farrell et al. ([12])	$2, 1, 1$	2586
this report	$2, 1, 1$	2586.2227
this report	$3, 2, 2$	2585.0189
this report	$4, 3, 3$	2585.0187
this report	$5, 4, 4$	2585.0187
this report	$6, 5, 5$	did not run

Table 1: Table of critical Rayleigh number for the Rayleigh-Bénard problem, where instability is always direct, ie. growth rates are all real. The notation $2, 1, 1$ refers to the element orders used for respectively the velocity, the pressure, and the temperature. All computations used a 50×50 mesh of uniform squares. The $6, 5, 5$ case failed to run due to an out-of-memory error.
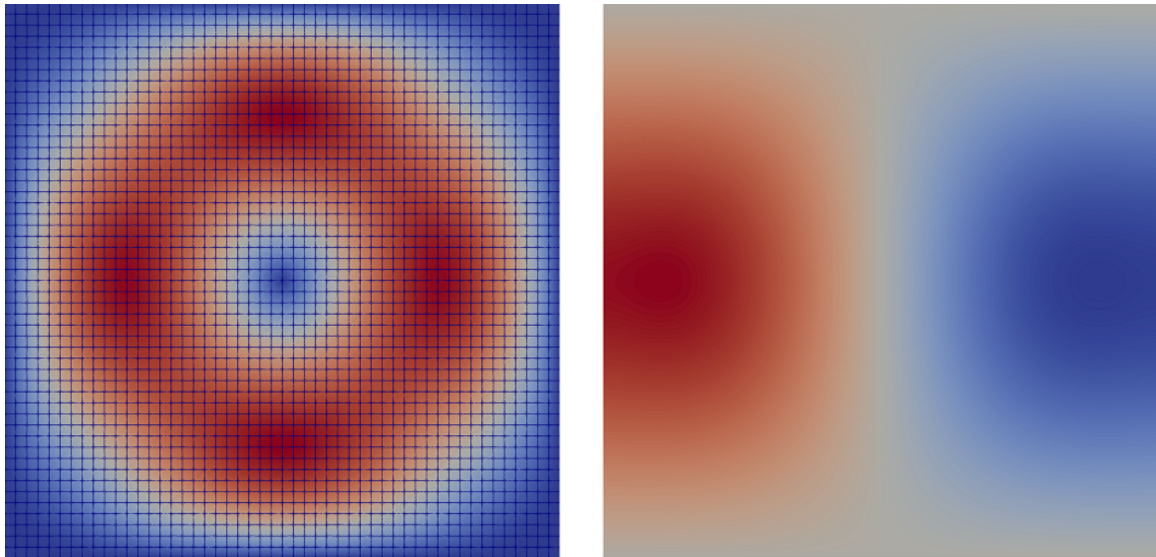

Figure 7: Velocity magnitude (left) and temperature profile of the instability mode found for Rayleigh-Bénard convection. Overall scale omitted as the eigenmode is defined up to a multiplicative factor. The computational mesh is overlaid on the velocity profile.

Author	element orders	Ra_c value	ω_c value
Winters ([13])	$2, 1, 2$	2.1092×10^6	1949.4
this report	$2, 1, 1$	did not converge	did not converge
this report	$3, 2, 2$	2.1103×10^6	1950.0
this report	$4, 3, 3$	2.1080×10^6	1949.1

Table 2: Table of critical Rayleigh number and corresponding oscillation angular frequency for the vertical convection problem with conducting floor and ceiling. The value from Winters is for the most accurate grid used for the first eigenvalue (28×28) and note that Winters used *discontinuous* first-order elements to discretize the pressure.

There are two choices of boundary conditions in the literature, with the use of insulating conditions on the floor and ceiling boundaries being the more common whereas the relatively early paper [13] used a conducting condition.

3.2.1 Conducting floor and ceiling

The vertical convection problem was treated in 1987 by Winters [13], who used a finite-element discretization with up to 32×32 grids of nine-noded (ie. second order) elements with a degree of refinement near the boundaries. The background steady-state and the eigenvalue problem were solved using the ENTWIFE finite-element code developed at Harwell running on a Cray S-2200.

A unit square cavity was used and the fluid had $\mathrm{Pr} = 0.71$, the value for air (due to the application of this problem to heat transfer across double glazing units). Note one detail here is the use of a linear temperature profile as a Dirichlet boundary condition $T = 1 - x$ on the floor and ceiling (called a conducting condition above).

In the FIREDRAKE implementation, the nontrivial background solution (Fig.8) was computed using a continuation method (see [14]) to reach a value known to be near the first Hopf bifurcation ($\mathrm{Ra} = 2 \times 10^6$ was used). A 40×40 mesh with boundary refinement was used.

The results (Table 2) show very good agreement with those of [13]. The instability mode is illustrated in Fig.9.

3.2.2 Insulating horizontal boundaries

The same problem with homogeneous Neumann (called insulating) boundary conditions on the floor and ceiling temperatures was treated by le Quéré and Behnia in [15], also using a Cray machine. The background solution is shown in Fig. 10, from which it is clear that there is a nontrivial flow at two of the corners, and the Griewank-Reddien analysis produced the first unstable mode shown in Fig.11, which shows that those interesting flows source the initial instability.

The choice of boundary conditions for the temperature can now be seen to have a very large effect, at least for $\mathrm{Pr} = 0.71$. Winters' [13] result is $Ra_c \approx 2.1 \times 10^6$ using the conducting boundary condition on the floor and ceiling of the cavity; by contrast, using insulating conditions on those
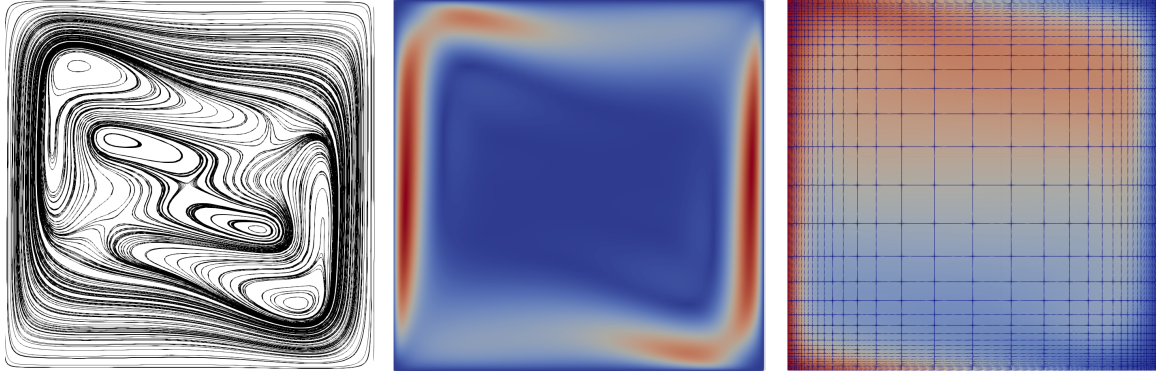
13

Figure 8: (L-R) Streamlines, velocity magnitude, and temperature profile near the first Hopf bifurcation (the actual value of Ra used is 2×10^6) for vertical convection using the conducting floor and ceiling boundary conditions. Overall scale omitted as the eigenmode is defined up to a multiplicative factor. The computational mesh is overlaid on the temperature profile.
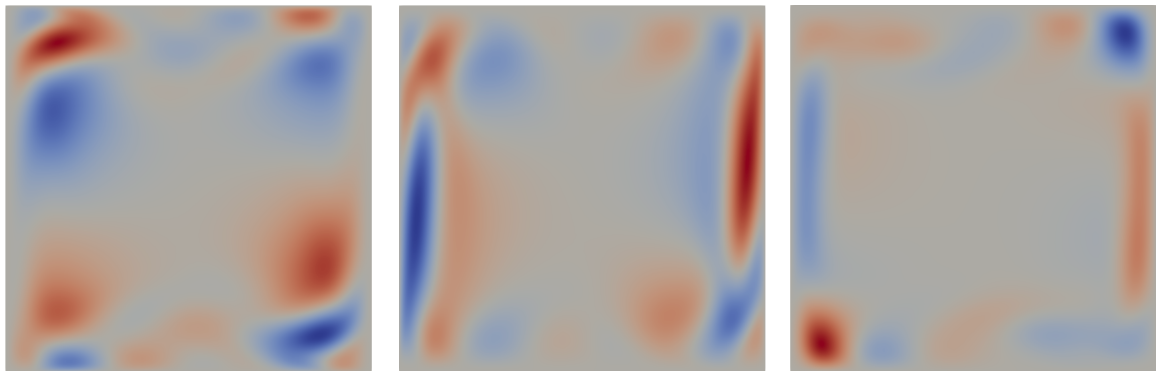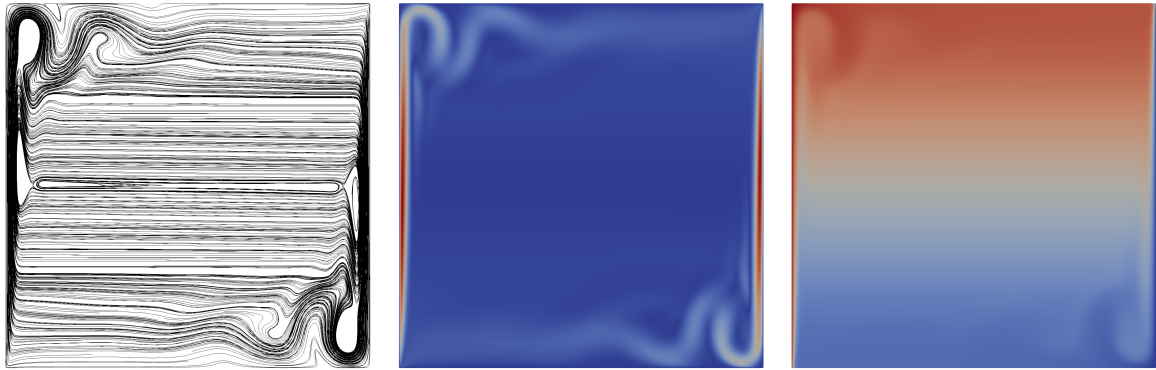

Figure 9: (L-R) Velocity components x and y and temperature profile of the first instability mode found for vertical convection using the conducting floor and ceiling boundary conditions. Overall scale omitted as the eigenmode is defined up to a multiplicative factor.

14

Figure 10: (L-R) Streamlines, velocity magnitude, and temperature profile of the background flow near the first Hopf bifurcation of the $\mathrm{Pr} = 0.71$ unit square vertical natural convection using the insulating floor and ceiling boundary conditions; $\mathrm{Ra} = 1.91 \times 10^8$.
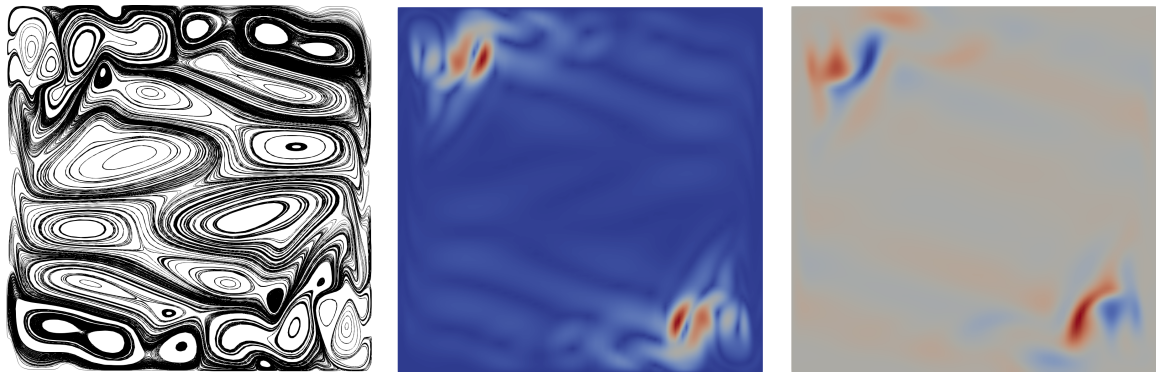

Figure 11: (L-R) Streamlines, velocity magnitude, and temperature profile of the first unstable mode of the $\mathrm{Pr} = 0.71$ unit square vertical natural convection using the insulating floor and ceiling boundary conditions; $\mathrm{Ra} = 1.91 \times 10^8$.

boundaries gives $Ra_c \approx 1.9 \times 10^8$, which is close to the le Quéré et al. [15] result that $Ra_c \approx 1.82 \times 10^8$. This represents two orders of magnitude difference in the value of Ra_c (and is another example of a well-insulated system retaining a steady flow better than an un-insulated one).

A Biot type boundary condition could be imposed with parameter α_B, eg. $(1 - \alpha_B)(T - T_0(x)) + \alpha_B \hat{\mathbf{n}} \cdot \nabla \cdot T = 0$ and presumably a UQ analysis would show a large sensitivity to the parameter α_B.

3.3   Vertical natural convection with $8 : 1$ aspect ratio

The paper by Zucatti et al. [16] treats the vertical natural convection problem in a tall ($8 : 1$ ratio) cavity, again air-filled: $\mathrm{Pr} = 0.71$. The floor and ceiling boundary conditions are insulating (but presumably this has less effect than for the unit aspect ratio case due to the relative shortness of the floor and ceiling boundaries here).

Using orders $3, 2, 2$ the Griewank-Reddien solver converges to $Ra_c = 304176.22$ with $\omega_c = 735.66$.

The results (12) can be compared with those illustrated for a value of Ra slightly above the Hopf bifurcation in [17] which were obtained using NEKTAR++, as well as those in Zucatti et al. [16].

3.4 Towards a phase diagram for vertical natural convection

An exploration of $(\mathrm{Ra}, \mathrm{Pr})$ space was performed in order to study the transition between steady laminar and non-steady oscillatory flows. A range of $\log_{10}\mathrm{Pr}$ from -2 to 2 is chosen (to make this more meaningful, a viscous oil such as glycerol has $\mathrm{Pr} \approx 10^3$, water ≈ 7, air ≈ 0.7, Mercury ≈ 0.015). For plasma, see [18, §2.3], the story is complicated by the presence of at least two different charged species, the Braginskii theory is argued as giving a Prandtl number of 0.23 based on perpendicular coefficients and 0.33 for parallel transport in the edge.

The set-up, including boundary conditions, is largely equivalent to that used in the paper by Farrell et al. ([12]) ie. a square cavity, but with a choice of conducting or insulating floor and ceiling boundary conditions as outlined in the preceding subsections. Note that the corresponding Rayleigh-Bénard problems were also studied and both cases showed a stability frontier independent of Pr. The parameter space was scanned by choosing a value for Pr and solving for the lowest eigenvalue at increasing values of Ra until a negative eigenvalue was discovered (the corresponding values of $(\mathrm{Ra}, \mathrm{Pr})$ were recorded). This simple line-based scanning technique was chosen because the initial implementation of the Griewank-Reddien solver seemed not particularly reliable, with convergence often not being achieved; the author has been informed [19] that the nonlinear system may require a fairly good initial guess of the critical value of the Rayleigh number in order to converge, so perhaps the best approach is to use the Griewank-Reddien solver to refine initial values obtained by a crude parameter scan.

The results of the parameter space scan are shown in Fig.13 for the case of the conducting floor and ceiling boundaries and Fig.14 for the insulating (adiabatic) floor and ceiling boundaries. (The results indicate that the departure from steady laminar convection occurs at much lower Ra for fluids like Mercury than for air / water / viscous oils, which is the case in reality.) Also shown in both cases is the result from the equivalent Rayleigh-Bénard problem in which the boundary conditions are basically rotated by $90°$ and in both Rayleigh-Bénard cases the stability frontier is independent of Prandtl number. Both graphs also include data points from the literature, with agreement being good for the conducting case (already seen in Table 2) and for both Rayleigh-Bénard cases. Agreement is less good for the value from [20] for the insulating case, which is more challenging due to the larger values obtained for the critical Rayleigh number. The insulating case is the more interesting, with the appearance of a very rapid change in $\mathrm{Ra_c}$ for $\mathrm{Pr} \approx 10^{0.21}$ and possibly a cusp at the end of this region (there may be additional cusps in the graph and indeed may be one or more in the conducting case). The region of rapid change is apparently associated to a rescaling of the flow (Fig.15). This feature may be present for other choices of the aspect ratio given that the feature is localized to the vertical walls with apparently little coupling between the walls. Note that the most interesting part of the curve, for $\mathrm{Pr} \in [0, 0.5]$, lies within the Pr range for probably the most important coolants used on Earth - air and water. (The apparent structure of this curve makes it an interesting subject for reduced-order modelling and surrogate construction.) It is clear that more data points are needed along with a proper analysis of convergence. Note the step size used in the horizontal scan of Ra at fixed Pr was $\frac{1}{64}$ in all cases - larger step sizes meant that the method would sometimes 'miss' a negative eigenvalue and find one at a larger
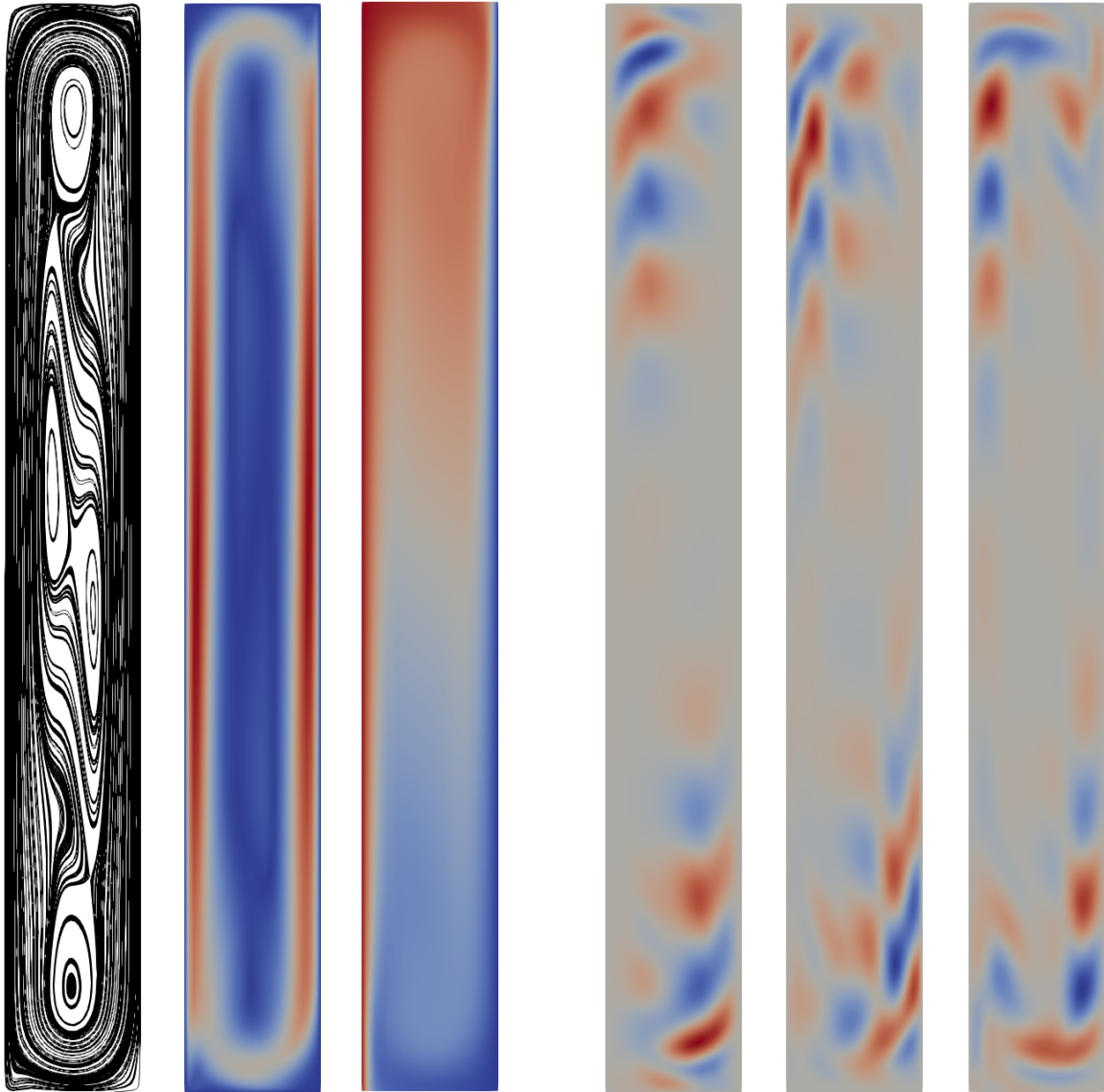
Figure 12: (L-R) Streamlines, velocity magnitude, and temperature profile very near the first Hopf bifurcation for the system in [16]. Overall scale omitted as the eigenmode is defined up to a multiplicative factor. The three plots on the right are x, y-components of velocity and T for the first eigenmode. The computational mesh is a 10×80 mesh of uniform squares.
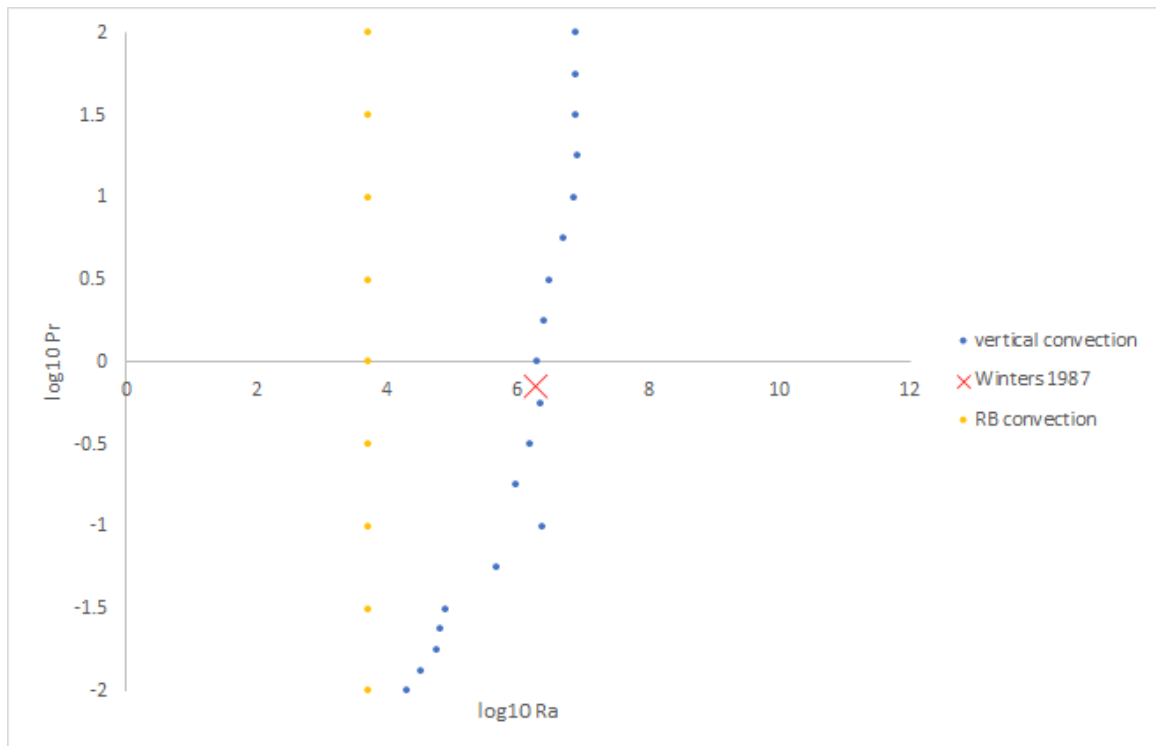
Figure 13: Phase diagram for vertical natural convection using the conducting floor and ceiling boundary conditions of [13] (the value for the first Hopf bifurcation from which is indicated by the red cross). The yellow points indicate where the same method has been applied to the first Hopf bifurcation of the Rayleigh-Bénard problem and the result in that case does not to depend on the value of the Prandtl number. In both cases, the time-stationary solution is stable to the left of the stability frontier and is assumed to remain unstable to the right of it.
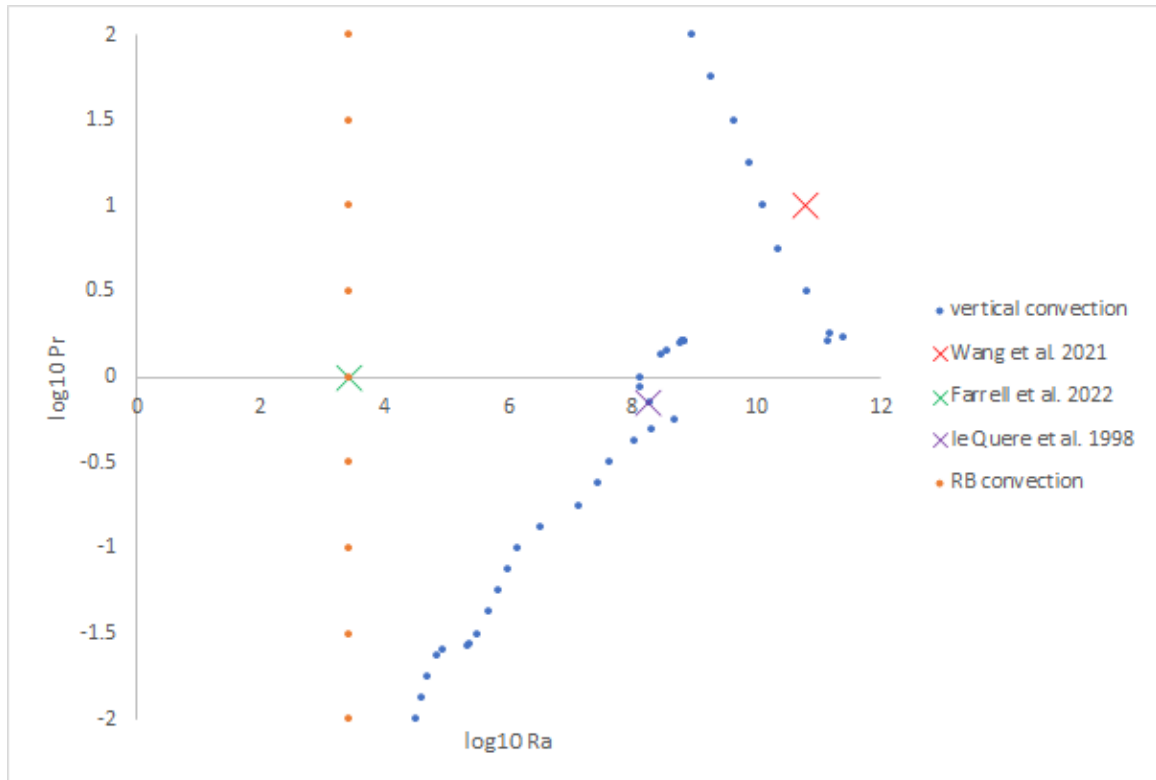
Figure 14: Phase diagram for vertical natural convection using the insulating floor and ceiling boundary conditions as in most of the literature, including [15]. The orange circles indicate where the same method has been applied to the first Hopf bifurcation of the Rayleigh-Bénard problem and the value of $\mathrm{Ra_c}$ there is seen to agree with the value of 2586 obtained in [12] (indicated by the green cross) and not to depend on the value of the Prandtl number. Two other values from the literature are plotted: The value at (non-log) $(10, 6 \times 10^{10})$ from [20], and the value at $(0.71, 1.82 \times 10^8)$ from [15].

Figure 15: Profiles of flow velocity magnitude at Ra_c for $\log_{10}\mathrm{Pr} = 0.205$ (left) and $\log_{10}\mathrm{Pr} = 0.225$ (right) for the insulating floor and ceiling boundary conditions. Note the abrupt change in scale of the corner flows between the two plots. The scale bars are not shown but the peak speed in the right-hand plot is ≈ 20 times that in the left-hand one. The difference in Ra_c between the two plots is more than two orders of magnitude.

value of Ra (perhaps a higher Hopf bifurcation) or would crash. Note the computations used the boundary-refined 40×40 mesh shown in the right-most plot of Fig.8 with element orders $5, 4, 4$ for velocity, pressure, and temperature. Fig.16 shows temperature and velocity profiles of background flows for a range of Pr values at or near first Hopf bifurcations for the insulating floor and ceiling boundary case. It is clear that the vicinity of $\mathrm{Pr} \approx 10^{0.25}$ is associated to very thin thermal boundary layers.

Note that this 'phase diagram' is a very good candidate for reduced-order modelling because a) it condenses a lot of simulation time into a single response surface (particularly true for the three-dimensional case) and b) the richness of physics in the problem and the nonlinearity make it very hard to predict without solving the full problem.

The author admits to not being a numerical analysis expert and plans to have the scripts used in this section reviewed by eg. the holder of the grant T/AW087/22 (numerical analysis). The author also offers apologies for including in a report on UQ results without error bars.

3.5 Three-dimensional convective heat transport

The 3-D version of the above problem is more challenging and will be run on Archer2. Studies are also being performed using NEKTAR++ - Fig.17 shows a preliminary output from a simulation on Archer2 where the 3-D geometry is a model for an actual fluid tank experiment being performed under the *SmalLab* programme. It is hoped that this investigation will provide a valuable addition to existing literature in addition to theoretical support for *SmalLab*.
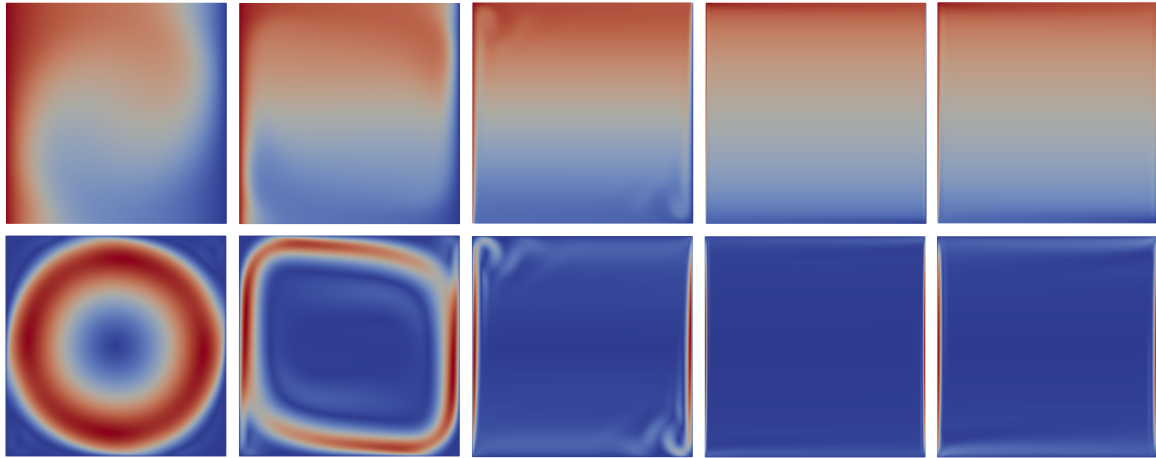
Figure 16: Temperature (top) and magnitude of velocity (bottom) profiles for $\mathrm{Pr} = -2, -1, 0, 1, 2$ (L-R) showing the background fields at or near first Hopf bifurcations for the insulating horizontal boundary case.
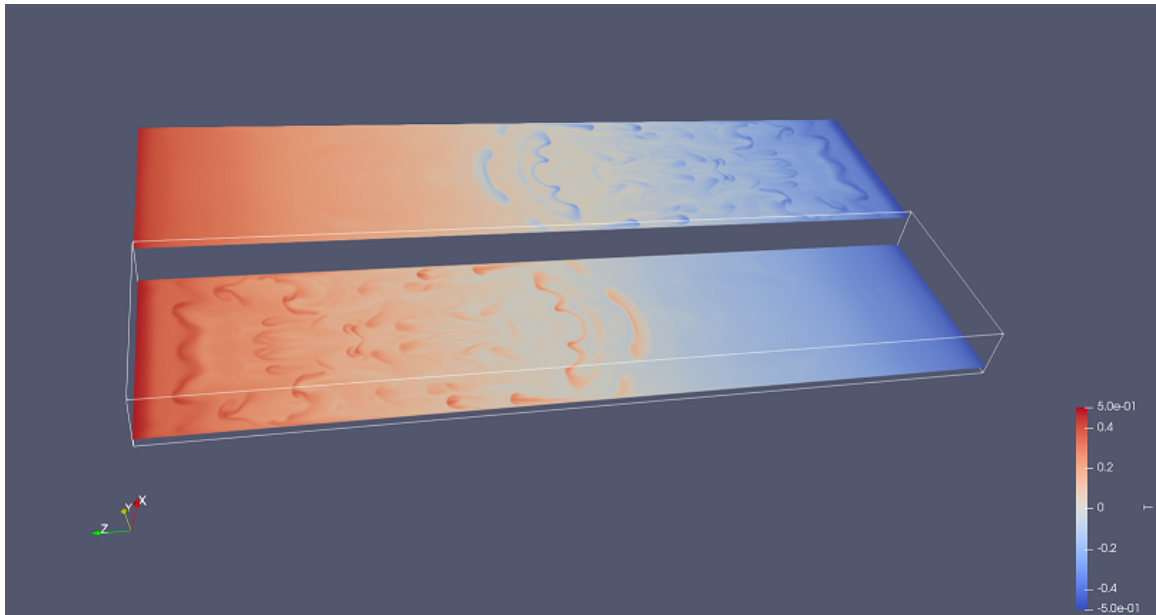

Figure 17: Temperature near hot and cold faces of 3-D convecting fluid tank (gravity acts in the negative z-direction and note the axes label on the figure). Obtained using NEKTAR++ on Archer2; the computational mesh comprises $189,000$ cuboidal elements.
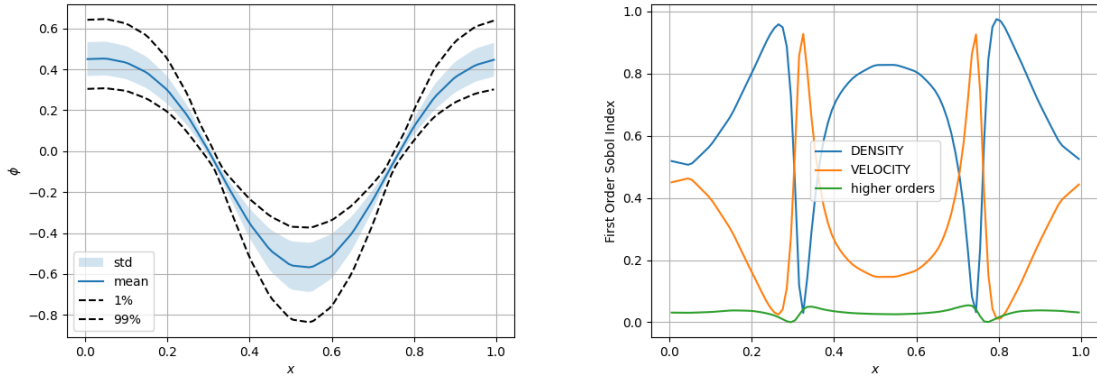
Figure 18: (Left) mean, variance and confidence intervals for the electrostatic potential ϕ evaluated using the PCE sampler. (Right) first-order Sobol indices for the potential.

4   Uncertainty quantification applied to *NESO-Particles*

It is expected that interesting and meaningful applications of non-intrusive UQ will be possible as the complexity of the code written under NEPTUNE develops; much focus in UQ is on analyzing systems with large numbers of control parameters, and once the atomic reactions, collision dynamics, and multiple species are included in the NEPTUNE code this will be a major topic of investigation. For now, a preliminary study has been set up, representing a successful initial integration of *EasyVVUQ*, *NESO-Particles* [21], and NEKTAR++ (which is used to perform the electrostatic solve in the particles code), and which is ready for future extension.

In this investigation, a polynomial chaos expansion (PCE) was fitted to the electrostatic potential generated by running a two-stream instability to a quasi-stationary state, for which it is known that the potential has an approximately sinusoidal form (see eg. Fig.6 of [22]). The PCE (which really does not have anything intrinsically to do with chaos) means expanding the output quantity of interest (QoI) in a set of polynomials in the input variables, and the latter are taken to be random variables with some probability distribution function (PDF); the nice property is the easy of computation of moments (mean, variance, etc.) as the cross terms cancel out by orthogonality. It is thus seen that the appropriate polynomial set is the Sturm-Liouville polynomial with weight function corresponding to the PDF of the random variables. The particular input parameters used here are the initial particle density and the stream velocity, both being taken to have uniform distributions (this means the polynomials of choice are the Legendre polynomials).

The first-order Sobol indices are also available in the example; these tell the how much of the variance in the QoI comes from each input.

Some details of the campaign were: 4×10^5 particles, particle density uniformly distributed on $[94.5, 115.5]$, initial velocity uniformly distributed on $[0.9, 1.1]$. The number of runs required for the campaign is defined by $N = (p+1)^d$ where p is the polynomial order ($p = 3$ was chosen, on the basis that it gave very similar outputs to $p = 2$) and $d = 2$ is the number of uncertain input parameters, so 16 runs were required for this exercise.

These scripts can be found in the GitHub repository [23].

5 Grantee work

Expertise in uncertainty quantification and reduced-order modelling is being provided to the NEP-TUNE project by the holder of the grant T/AW085-21, University College London, via the AQUIFER project (the acronym derives from Advanced Quantification of Uncertainties In Fusion at the Ex-ascale with model order Reduction)). That grantee is also responsible for the SEAVEA project [24] (the acronym stands for Software Environment for Actionable and VVUQ-evaluated Exascale Applications) under which is developed and maintained the *SEAVEA Toolkit*, a significant body of open-source software for uncertainty quantification; this will be described briefly. Note much of this software was formerly under the guise of the *VECMA Toolkit*.

A simple summary of the components of the *SEAVEA Toolkit* is:

- *EasyVVUQ* - provides tools for non-intrusive uncertainty quantification, including the construction of polynomial chaos surrogates and the calculation of Sobol indices.

- *MUSCLE3* - A framework for coupling codes and propagating uncertainty through the coupling.

- *FabSim3* - a framework for automating UQ workflows on HPC.

- *QCG-Client and Broker* - manages different job types, including complex workflows using supercomputers.

- *QCG-PilotJob* - tool enabling the submission of large numbers (eg. 10^8) of individual jobs to a supercomputer.

- *QCG-Now* - aims to enable getting quick and convenient use of a supercomputer.

- *EasySurrogate and MOGP* - tools for constructing cheaper surrogate models; MOGP (for Multi-Output Gaussian Process) computes Gaussian process surrogates.

The toolkit is being actively developed and some additions have been made to target specific problems raised by UKAEA eg. surrogates for models with discontinuous response surfaces via the simplex-stochastic correlation method as explained in [25].

It is notable that many of the VVUQ tools in *EasyVVUQ* deal only with forward uncertainty propagation, ie. they do not work in cases where there is two-way coupling between models.

A particle filter-based data assimilation package, *ParticleDA.jl* [26], was released during 2022 and is currently being integrated with the above tools. An initial version, which provides data assimilation capability linked to the other capabilities of the *SEAVEA Toolkit*, can be found at [27].

The grantee has implemented a plug-in for *FabSim3* which uses as target problem a choice of two-dimensional and three-dimensional fluid convection problems in NEKTAR++. This facilitates applying the SEAVEA toolkit to NEPTUNE -specific problems.

Two hackathons were held (24 June and 8-9 December 2022). The first of these was attended remotely by ET and Owen Parry of UKAEA and focussed on running *Fab*NEPTUNE both locally and on Archer2. The second was held at UCL; authors ET and SP attended in-person and focussed on integrating *EasyVVUQ* with *NESO-Particles*. In December 2022, James Cook gave a presentation at the SEAVEA Applications Meeting, which was attended by other UKAEA personnel, on the topic of FEM-Particle Coupling with *NESO-Particles* being the main focus. A high level overview of the implementation of *NESO-Particles* was given: the L2 Galerkin projection of particle quantities to a fluid representation of the density of that quantity; the capability to store arbitrary data on particles; the ideas behind how particle movement is formed between cells and across MPI ranks; and finally favourable scaling of both local and global particle transfer across the MPI domain is shown.

The grantee has performed an initial comparison between linked and deep Gaussian Process approaches for an example problem. The grantee has also performed a study of data assimilation as applied to the outputs of a nonlinear ODE system containing two time-scales - this model replaces actual physical data that, due to delays in getting the *SmalLab* experimental campaign working, is not yet available.

The grantee has provided HPC allocations including Archer2 and also the future prospect of Frontier and its testbed proxy Crusher, the latter of which will be exploited as soon as a scaleable NEPTUNE GPU code is available.

6 Summary

A computationally-cheap one-dimensional system of a reduced convection model coupled to a diffusion model was demonstrated and was shown to exhibit the phenomenologically-plausible behaviour of more insulation suppressing chaotic behaviour. It is worth noting however that the models assume a uniform temperature of insulator, which may be difficult to achieve in practice (D. Buta, private communication). A two-dimensional case of vertical natural convection was studied and the boundary in parameter space between steady laminar flows and oscillatory flows, which is the start of the transition to turbulence, was uncovered for two choices of boundary conditions on the horizontal boundaries of the domain. The ensemble UQ package EASYVVUQ was applied to the NEPTUNE particles code NESO-PARTICLES. The work of the holder of grant T/AW085/21 on UQ and reduced-order models was briefly summarized.

Acknowledgement

References

[1] F. Wilczynski, D.W. Hughes, W. Arter, and F. Militello. Onset of interchange instability in a coupled core-SOL plasma. *Physics of Plasmas*, 27(7):072508, 2020.

[2] Lorenz E.N. Deterministic nonperiodic flow. *J. Atmos. Sci. 20*, pages 130–141, 1963.

[3] Dullin H., Schmidt S., Richter P.H., and Grossmann S.K. Extended phase diagram of the Lorenz model. *International Journal of Bifurcation and Chaos Vol.17 No.09, pp.3013-3033*, 2007.

[4] N. Gershenfeld. *The Nature of Mathematical Modelling*. Cambridge University Press, 1999.

[5] S. Grossmann and D. Lohse. Scaling in thermal convection: a unifying theory. *Journal of Fluid Mechanics*, 407:27–56, 2000.

[6] Florian Rathgeber, David A. Ham, Lawrence Mitchell, Michael Lange, Fabio Luporini, Andrew T. T. Mcrae, Gheorghe-Teodor Bercea, Graham R. Markall, and Paul H. J. Kelly. *Firedrake*: automating the finite element method by composing abstractions. *ACM Trans. Math. Softw., 43(3):24:124:27, 2016. URL: http://arxiv.org/abs/1501.01809, arXiv:1501.01809, doi:10.1145/2998441.*, 2015.

[7] Scalable Library for Eigenvalue Problem Computations. `https://slepc.upv.es/`. Accessed: September 2022.

[8] Griewank A. and Reddien G. The calculation of Hopf points by a direct method. *IMA J. Numer. Anal., Vol.3, pp.295-303.*, 1983.

[9] Boulle N., Farrell P.E., and Rognes M.E. Optimization of Hopf bifurcation points. *arXiv preprint arXiv:2201.11684*, 2022.

[10] S. Chandrasekhar. *Hydrodynamic and Hydromagnetic Stability*. Clarendon Press, 1961.

[11] J.M.T. Thompson and H.B. Stewart. *Nonlinear Dynamics and Chaos, 2nd Edition*. John Wiley & Sons Inc, 2002.

[12] N. Boullé, V. Dallas, and P. E. Farrell. Bifurcation analysis of two-dimensional rayleigh-bénard convection using deflation. *Phys. Rev. E*, 105:055106, May 2022.

[13] Winters K.H. Hopf bifurcation in the double-glazing problem with conducting boundaries. *Transactions of the ASME 894 / Vol.109, November 1987.*, 1987.

[14] Arter W., Parry O., and E. Threlfall. Finite element models: complementary actions 3. Technical Report CD/EXCALIBUR-FMS/0074, UKAEA Project Neptune.

[15] le Quéré P. and Behnia M. From onset of unsteadiness to chaos in a differentially heated square cavity. *J. Fluid Mech. (1998) vol.359 pp81-107*, 1998.

[16] Zucatti V., Lui H.F.S., Pitz D.B., and Wolf W.R. Assessment of reduced-order modelling strategies for convective heat transfer. *Numerical Heat Transfer: Part A: Applications 77:7.*, pages 702–729, 2020.

[17] E. Threlfall. Finite element models: complementary actions 2. Technical Report CD/EXCALIBUR-FMS/0064, UKAEA Project Neptune, 2022. `https://github.com/ExCALIBUR-NEPTUNE/Documents/blob/main/reports/ukaea_reports/CD-EXCALIBUR-FMS0046-M6.2.pdf`.

[18] W. Arter et al. Equations for EXCALIBUR/NEPTUNE Proxyapps. Technical Report CD/EXCALIBUR-FMS/0021-1.26-M1.2.1, UKAEA, 1 2023. `https://github.com/ExCALIBUR-NEPTUNE/Documents/blob/main/reports/ukaea_reports/CD-EXCALIBUR-FMS0021-1.26-M1.2.1.pdf`.

[19] Farrell P.E. Private communication, 2023.

[20] Wang Q., Liu H-R., Verzicco R., Shishkina O., and Lohse D. Regime transitions in thermally driven high-Rayleigh number vertical convection. *J. Fluid Mech. (2021) Vol.197 A.6 doi:10.1017/jfm.2021.262*, 2021.

[21] NESO-Particles code repository. `https://github.com/ExCALIBUR-NEPTUNE/NESO-Particles`. Accessed: September 2022.

[22] E. Threlfall and W. Saunders. Support high-dimensional procurement. Technical Report CD/EXCALIBUR-FMS/0066, UKAEA Project Neptune, 2022. `https://github.com/ExCALIBUR-NEPTUNE/Documents/blob/main/reports/ukaea_reports/CD-EXCALIBUR-FMS0066-M4.1.pdf`.

[23] NESO-UQ code repository. `https://github.com/ExCALIBUR-NEPTUNE/NESO-UQ`. Accessed: March 2023.

[24] SEAVEAtk. `https://www.seavea-project.org/seaveatk/`. Accessed: March 2023.

[25] Edeling W.N, Dwight R.P., and Cinella P. Simplex-stochastic collocation method with improved scalability, 2016.

[26] ParticleDA.jl. `https://github.com/Team-RADDISH/ParticleDA.jl`. Accessed: March 2023.

[27] FABParticleDA. `https://github.com/djgroen/FabParticleDA/tree/master`. Accessed: March 2023.